Spectral reflectance estimation from Transverse Field Detectors responses

Miguel A. Martinez, Eva M. Valero, Javier Hernandez-Andres; University of Granada; Granada, Spain; Giacomo Langfelder; Politecnico di Milano, Milano, Italy

Abstract

The main aim of this study is to investigate which would be the best algorithm for spectral estimation from Transverse Field Detectors (TFD) sensor responses. We perform a quality check of the estimation accuracy of five different algorithms, most of which are recent proposals. Some modifications are introduced as well in their implementation to simplify calculations or to increase the performance (see subsection Spectral estimation algorithms for details). The results obtained have allowed us to introduce relevant suggestions for enhancing the TFD sensor performance for their use in multispectral capture devices. This work paves the way for the practical development of a fully automatic multispectral device based on sensors with reconfigurable responsivities.

Introduction

Multispectral imaging deals with retrieving spectral information for each pixel of an image, and it has been a rather active research field in the last 10-15 years [1]. The range of possible applications is quite wide and covers, among others, medical imaging [2], food industry [3], remote sensing [4], and military purposes [5]. New applications are also emerging at a fast pace. A typical multispectral device captures the image with a reduced number of sensors, and then uses an algorithm to estimate the spectral information from the camera responses [6]. Ultra and hyperspectral systems [7] don't estimate the spectra. They measure them, but they are usually more expensive and complex than multispectral devices. Many efforts have been dedicated to try to achieve full spatial and spectral resolution with one single sensor offering a fast response and high accuracy [8]. The Transverse Field Detectors [9],[10] are one of the most recently developed devices with potential applications in multispectral imaging. These devices are based on filterless colour sensitive pixels. The working principle takes advantage of the wavelength-dependent properties of light absorption in Silicon. The different wavelengths penetrate the Silicon substrate reaching different depths. Then, the photocarrier collection can be organized so that each single pixel can provide responses to several channels at the same time (usually, 3 channels are collected for each single pixel, but there can be potentially even up to 5 channels responding to the incoming light). One additional fundamental advantage of this technology is that it can exploit the tuneability of the electric fields applied. Thereby it offers reconfigurable spectral responsivities simply by applying different biasing voltages to the pixel, without the need of moving mechanical components. This emerging technology is then very interesting as a candidate for achieving full resolution multispectral capture. The reconfigurable responsivities of the TFD sensors have quite unique features. The design of a multispectral capture system including these special kind of sensors must include a wide set of previous computational simulations to study the influence of several factors on the spectral accuracy of the device, like the spectral estimation algorithm used to obtain the colour signals or reflectances from the sensors responses. Several studies offer data on comparative performance of spectral estimation algorithms for different multispectral systems [11],[12],[13], but none of them have used reconfigurable or TFD responsivities so far.

Methods

This study is based on simulation of the sensor responses of a multispectral device equipped with a TFD sensor. We first will find the optimal channels for our system in subsection "TFD sensor responsivities", then describe the computational calculation of sensor responses (including additive noise) and the spectral database built for assessing spectral estimation accuracy in subsection "Simulated camera responses and spectral data". Some insight into the algorithms underlying ideas and their implementations is given in subsection "Spectral estimation algorithms". The quality indices used are described in subsection "Spectral recovery quality indices".

TFD sensor responsivities

We explained previously that each single pixel of the sensor offers three channel responses (R, G and B), which are reconfigurable by changing the biasing voltage. This biasing voltage can be changed before each capture. One of the first issues that we have to consider is how many channels are going to be included in our multispectral system. The number of channels determines the number of shots for each capture. For instance, if we are designing a single-shot multispectral then we would have three channels (the three corresponding to R, G and B for each pixel). Then, if we need to add additional channels, we have to tune the spectral responsivities of the TFD and so change the applied bias voltage and take two shots for each capture, allowing for up to six channel responses. We have to consider a trade-off between the potential advantage of using additional channels and the disadvantage of adding more shots to each capture. As a starting point, the spectral responsivities of eight different biasing conditions (each corresponding potentially to one shot and three different channels) were simulated using a range of maximum applied voltages $\leq 9V$ to cope with typical sensors voltages. The simulated spectral responsivity curves are shown together with several experimental ones, obtained on a new prototype structure, in figure 1. We can see that there is a relatively good agreement between the simulated and the experimental responsivities shown. Among these responsivities, we selected the group of three RGB channels (one shot approach) offering the best estimation quality. We used for this purpose the least computationally demanding estimation algorithms, which were the pseudoinverse and matrix R (see details in subsection Spectral estimation algorithms) and the spectral database described in subsection Simulated camera responses and spectral data. We added then an additional channel by testing all the rest of the remaining

21 channels one by one and evaluating the spectral estimation accuracy, and finally selected the additional channel that offered the best performance. So far we have then a two-shots (as we have to change voltage once to introduce the additional channel) but four-channels multispectral capture device. At least for the present implementation, using all the three channels in the second shot (up to six globally) resulted in a decrease in estimation quality, so only the green channel of the second shot (offering the best performance) was selected. The corresponding normalized spectral responsivities chosen as sensors of the multispectral device are shown in figure 2.

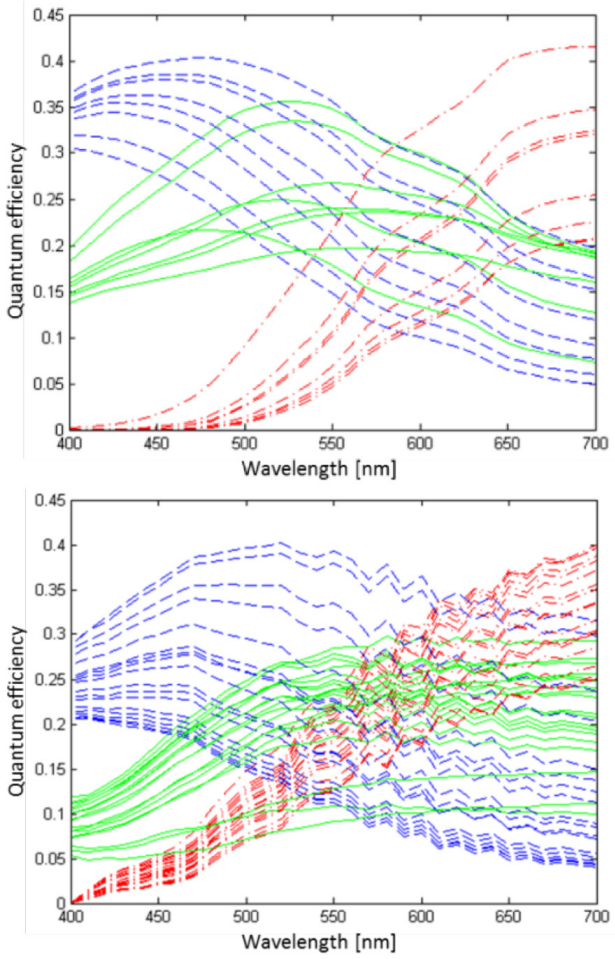

Figure 1. *(Top) simulated RGB spectral responsivities corresponding to different applied biasing voltages; (Bottom) experimental spectral responsivities obtained on a prototype TFD pixel built in a CMOS standard 150nm technology. Note that for each biasing condition, the overall quantum efficiency for each pixel is the sum of the corresponding RGB efficiencies*

Simulated camera responses and spectral data

We have calculated the camera responses using the spectral responsivities and the color signals corresponding to the product of the reflectance set by the SPD of the illumination, as explained in eq. 1:

$$\rho = R^T E + \sigma \tag{1}$$

Where ρ represents the sensor responses to the color signal E, and R is the matrix of spectral responsivities of the sensors, which is transposed as indicated by the T superindex. σ represents the additive noise. When noiseless camera responses are simulated, $\sigma = 0$. Therefore, for noiseless simulations, each color signal will have 4 sensor responses. For noisy camera responses, a normal distribution of σ-values is calculated for each noise-free response. This distribution is centered in the noise-free camera response, and its standard deviation is calculated as shown in eq. 2:

$$\sigma_i = 0.01 \cdot r_{iw} \sqrt{\frac{r_i}{r_{iw}}} \tag{2}$$

Where r_{iw} is the camera response for a perfect white under the same illumination and r_i is the noise-free camera response. We have simulated intensity dependent noise (shot noise and flicker noise). The value 0.01 was selected because it simulates optimally an existing imaging system. Quantization noise is also introduced (using 12 bits per channel, which is a typical value for a commercial digital camera). Dark current noise can be avoided subtracting the dark image to each sample image, and thermal noise can be reduced down to negligible values cooling the camera, so these two noises are not simulated. In this study, we have used as spectral data a reflectance set designed to allow for generalization of results. It is composed of 160 reflectances which were chosen among different publicly available databases corresponding to: 60 from urban scenes and rural scenes [14], 20 from Munsell book of colors, 30 from Vhrel's database [15] and 50 from the Color Checker DC (Gretag Macbeth GmbH, Germany). We have used the standard illuminant D65 for computation of the color signals. The samples have a quite regular distribution in the $L^*a^*b^*$ color space.

Spectral estimation algorithms

Five different algorithms have been selected which are representative of different strategies for estimating spectral reflectance from few sensor responses. We have used the following criteria for the selection of algorithms: amount of data needed as input (some of them need the spectral responsivities of the sensors, some only require a training set, others both) and absence of use of dimensionality reduction techniques, which would require additional reflectance sets to work optimally. The final selection of algorithms includes the pseudoinverse [16], [17], kernel [11], Projection onto convex sets (POCS) [18], MatrixR, and radial

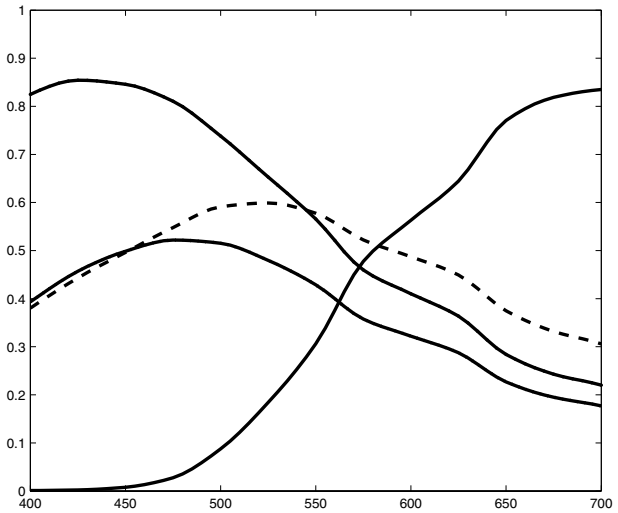

Figure 2. *Optimal normalized 4 sensitivities selected against wavelength (nm). Normalization is done to set as 1 the maximum value out of all 8 TFD set ups.*

basis functions neural networks (RBFNN) [19]. Some details of the implementation for each algorithm are explained below. We have used the leave one out cross validation method [20] for the selection of samples forming the training and test sets. It is an iterative method, which takes out one reflectance from the set of 160, as test set, while the remaining 159 reflectances are the training set. So the reflectance that is estimated is never included in the training set.

Pseudoinverse

This algorithm uses as input the color signals of the training set and the sensor responses of the training and test sets. The first step is to build a transformation matrix D as eq. 3 shows:

$$D = C_T \times \rho_T^+ \tag{3}$$

Where C_T is the set of color signals corresponding to the training set and ρ_T^+ is the pseudoinverse matrix of the sensor responses for the training set. Finally, the estimated color signal C is obtained as eq. 4 shows:

$$C = D \times \rho \tag{4}$$

Where ρ is the vector with sensor responses for the test set. The estimated reflectance is obtained by discounting the illumination from the color signal C.

MatrixR

This algorithm is based in the combination of the Wyzsecki hypothesis and the matrix R theory. It involves the calculation of two transformation matrices, one spectral transformation M_s and one colorimetric transformation M_c. The recovered color signal is calculated as eq. 5 shows:

$$C = [A \times (A' \times A)' \times T_p] + [(I - R) \times N] \tag{5}$$

Where the first term of the sum corresponds to the fundamental stimulus N^* and the second to the metameric black B. A is the matrix of color matching functions (CMF) of the CIE 1931 2 deg. standard observer. T_p is the matrix with the predicted tristimulus values, calculated as eq. 6 shows:

$$T_p = [T \times \rho_L^+] \times [(\alpha \times \rho_T + \beta)^\gamma] \tag{6}$$

Here the first term corresponds to the colorimetric transformation M_c and the second one to the corrected sensors' responses for the training set (ρ_L) after applying a gain-offset-gamma (GOG) model. This way of computing M_c is different from the original proposal of the algorithm and it offers the advantage of being simpler and making the algorithm to gain in generality. The matrix R is calculated as eq. 7 shows:

$$R = A \times (A' \times A)^{-1} \times A' \tag{7}$$

And finally N is the starting value spectrum for each estimate sample and it is calculated as eq. 8 shows:

$$N = M_S \times \rho \tag{8}$$

Where the M_s matrix is equal to D in the pseudoinverse algorithm and ρ is the matrix of sensors' responses for the test set. In this algorithm the parameterization of α, β and γ plays an important role in order to get optimal performance. Thus, an optimization procedure is implemented to check all possible combinations of values within a given range and obtain the best combination of parameters minimizing a combined spectral and colorimetric distance measure explained after. This optimization procedure was not implemented in the version of matrix R used in a preliminary study not including TFD sensors [20].

Kernel

This algorithm estimates directly reflectances instead of color signals. The first step is to calculate the Gaussian kernel matrices K and κ according to eq. 9:

$$K_{jm} = exp(-\frac{(C_{Tj} - C_{Tm})' \times W' \times W \times (C_{Tj} - C_{Tm})}{2\sigma^2}) \tag{9}$$

Where C_{Tj} is a column vector formed by the color signal corresponding to sample j of the training set, and W is a matrix containing the spectral responsivities of the sensors. The parameter σ is the effective area of the kernel, and its optimal value was 4.9×10^{-11} for our particular data set. It was obtained after some brute-force optimization process as the one giving the best estimation quality. The second kernel function κ is calculated for each estimated sample i as eq. 10 shows:

$$\kappa_j = exp(-\frac{(\rho_j - \rho_i)' \times (\rho_j - \rho_i)}{2\sigma^2}) \tag{10}$$

This kernel matrix creates a feature space with the same dimension as the number of samples. Then, the estimated reflectance for sample i is calculated as eq. 11 shows:

$$R_k = R_T \times (K + \gamma I)^{-1} \times \kappa' \tag{11}$$

The parameter γ is introduced in the recovery equation to prevent instabilities in the matrix inversion. Its optimal value was found to be 4.7×10^{-5}.

POCS

This algorithm works iteratively by computing normalized projections of the initial estimates onto the responsivities of the sensor set (multiplied by the illumination SPD), and correcting the initial estimate each step by decreasing the difference between this projection and the sensor response, maintaining a positivity and a smoothness constraints. The smoothness constraint has been introduced by us to improve the quality of the estimations. To obtain the estimated spectral reflectance we compute the factor G_j as shown in eq. 12:

$$G_j = \frac{F_i' \times W_{SPD_j} - \rho_{ij}'}{N_j} \cdot W_{SPD_j}' \tag{12}$$

Where ρ_{ij} is the sensor response corresponding to the sample being estimated (i) for sensor j, F_i is the starting value or initial estimate, W_{SPD_j} is a matrix containing the product of the spectral responsivities by the illumination SPD, and N_j is a vector containing the square Euclidean norm of matrix W_{SPD_j}. Then, we correct the initial estimate F_i by subtracting G_j and introduce the positivity and smoothness constraints. The number of iterations is the only parameter we can vary in this implementation of the algorithm. We have found an optimal value of 412.

RBFNN

This algorithm creates a neural network with one hidden layer and trains it with the training set of color signals in order to recover also a color signal. The training is done by minimizing the mean squared error (MSE) adding neurons to the network. The activation function of each neuron is a Gaussian function. The parameters to be set here are maximum number of neurons to be added, goal MSE and spread of the network, with optimal values found of 40, 0 and 40 respectively. The RBFNN algorithm has the drawbacks of being very sensitive to an adequate selection of the training set and also of being somewhat computationally demanding, as it involves an iterative training step.

Spectral recovery quality indices

We used three metrics to analyze the quality of the spectral estimates obtained by the different algorithms. Two of them are based on spectral similarity between the original and estimated samples (the root mean square error or RMSE, and the goodness-of-fit coefficient or GFC [21]), and one of them is based on visual perception (the CIELab Color difference equation or ΔE^*_{ab} using D65 as reference white and the CIE 1931 standard colorimetric observer). The RMSE index focuses on absolute differences between the original and estimated sample reflectance, and so is not independent of scale factors. In the best case it equals 0.

$$RMSE = \sqrt{\frac{1}{n}\sum_{j=1}^{n}(E(\lambda_j) - E_R(\lambda_j))^2} \tag{13}$$

The GFC quality index is the cosine of the angle formed by the two samples in the high-dimensional vector space of spectral signals. The closer the GFC is to unity, the better the estimation quality of the sample. The GFC index is independent of scale factors; so two samples differing only in scale but not in shape would result in a GFC of 1.

$$GFC = \frac{\sum_{j=1}^{n} E(\lambda_j)\cdot E_R(\lambda_j)}{[\sum_{j=1}^{n}[E(\lambda_j)]^2]^{\frac{1}{2}}\cdot[\sum_{j=1}^{n}[E_R(\lambda_j)]^2]^{\frac{1}{2}}} \tag{14}$$

The ΔE^*_{ab} is just the Euclidean distance between both samples within the CIELab color space. There are newer color difference formulae recommended by the CIE, like CIE94 or CIEDE2000. We have chosen this color difference equation because the aim in this work is to compare between different algorithms so the choice is not really critical in this case, and this measurement is widely used in the literature. An additional metric has been used for the optimization process. It's the combined spectral and colorimetric metric (CSCM) [21].

$$CSCM = \ln(1+\alpha\cdot(1-GFC)) + (\beta\cdot\Delta E^*_{ab}) \tag{15}$$

For a perfect match, this parameter equals 0, and we can control the weight of the spectral and colorimetric metrics varying the parameters α and β. We have set these values to $\alpha = 1000$ and $\beta = 10$.

Results

Noiseless camera responses

In table 1 we show the average and standard deviation of the quality indices for the 160 samples for the different algorithms.

Table 1: Noiseless results. Standard deviation in parenthesis.

Algorithm	GFC	RMSE	ΔE^*_{ab}
Pseudoinverse	0.9979 (0.0026)	0.0286 (0.0131)	3.05 (2.40)
MatrixR	0.9981 (0.0022)	0.0289 (0.0137)	2.03 (1.36)
RBFNN	0.9981 (0.0051)	0.0251 (0.0131)	2.76 (2.59)
POCS	0.9984 (0.0020)	0.0250 (0.0132)	2.09 (1.89)
Kernel	0.9984 (0.0026)	0.0237 (0.0134)	1.69 (1.76)

The best results are those of Kernel while the worst are those of Pseudoinverse for GFC and ΔE^*_{ab} and Matrix R for RMSE. The quality of the estimations can be considered acceptable for spectral indices and also for color differences in the best cases.

Noisy camera responses

In table 2, we show the results corresponding to the average and standard deviation of the 1600 recoveries done for each algorithm (10 for each reflectance with different values of σ equally spaced in the noise distribution). As expected, the recovery quality decreases when compared to noise-free data.

Table 2: Noisy results. Standard deviation in parenthesis.

Algorithm	GFC	RMSE	ΔE^*_{ab}
Pseudoinverse	0.9941 (0.0064)	0.0497 (0.0216)	9.37 (7.26)
MatrixR	0.9962 (0.0041)	0.0487 (0.0233)	4.57 (4.0769)
RBFNN	0.9941 (0.0337)	0.0473 (0.0238)	8.2807 (9.5163)
POCS	0.9959 (0.0049)	0.0416 (0.0192)	5.7098 (4.1218)
Kernel	0.9965 (0.0083)	0.0385 (0.0217)	4.3313 (3.2500)

Once more, the best results are those of Kernel, and the worst those of pseudoinverse. The algorithm that has registered the highest loss in the quality of the recovered signals is pseudoinverse. This shows that it is the least robust against noise. We have to consider also that there's no possible room for improvement in these results because the algorithm is not parametric. Also the matrix R and the RBFNN have shown less robustness against noise than POCS and kernel. We must take into account for the analysis of these results the fact that the weight given to the 10 noisy responses in the calculation of the recovery quality indices is the same for all levels of noise; instead, for a real system, the likeliness of getting noisy camera responses in the extremes of the distribution would be rather low. So in our computations we have designed almost a "worst case" scenario. We expect that using real sensor responses would offer better estimation quality than our noisy data simulations. However, we are unable to put this assertion to the test because the sensors are still in an early stage of development. In the near future, we plan to use the real responsivities data shown in figure 1 (bottom) with simulated noise to compare the spectral estimation performance data with those obtained using the simulated responsivities, which are presented in this study. In figure 3 we can see the comparison of noiseless and noisy results for the ΔE^*_{ab}.

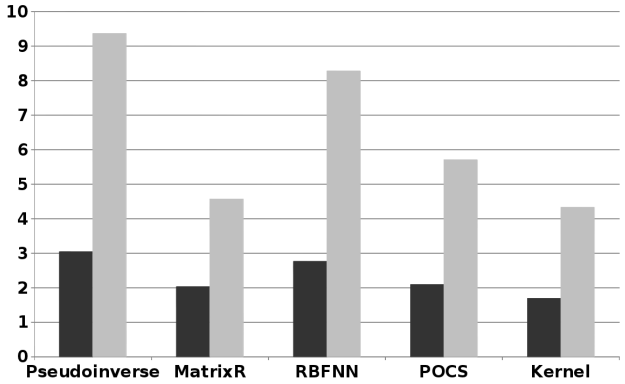

Figure 3. *Comparison of ΔE^*_{ab} for noiseless and noisy sensors. The darker bars correspond to noiseless sensors' responses*

We can see that the worst behavior when noise is introduced corresponds to Pseudoinverse, as commented earlier, and to RBFNN. This can be explained because the RBFNN algorithm

tries to map directly camera responses onto spectral data, and this gets increasingly difficult if the noise increases. The matrix R algorithm behaves better regarding the colorimetric index because it is designed specifically to obtain good colorimetric quality for its estimations. In figure 4 we show two examples of the best recoveries for the noisy case and two examples of the worst.

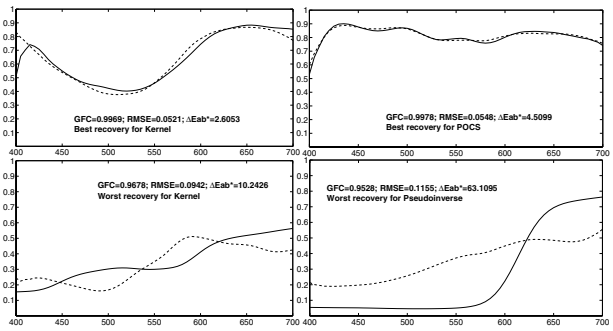

Figure 4. *Examples of best and worst reflectance recoveries against wavelength (nm).*

The best recoveries were found for the sensors' responses close to the noise-free case, and the worst recoveries to those values in the extremes of the noise distribution. As expected, the higher the noise the worst the recovery accuracy.

Comparison with narrower sensitivities

It was found that the results with TFD sensitivities for the noisy case are not very good especially regarding the color difference index. A further study was done with the same set of reflectances for the set of six narrow sensitivities used in [23]. Since kernel provided the best performance, in table 3 the results presented correspond to this algorithm for both the noiseless and noisy cases.

Table 3: Noisy results. Std. in parenthesis.

Metric	Noiseless	Noisy
GFC	0.9987 (0.0023)	0.9985 (0.0025)
RMSE	0.0214 (0.0155)	0.0266 (0.0161)
ΔE^*_{ab}	0.2033 (0.2583)	0.7324 (0.3768)

It can be seen that for these sensitivities the recoveries are well below the tolerance limit for color difference and spectral indices, even in the noisy case. This points out the fact that narrower responsivities are better able to separate the samples in the sensor response space and so the algorithms can perform better. Improvements in the spectral recovery performance are thus expected also for the TFD by combining the sensor responsivities with external filters like UV-IR filters (always part of a digital camera, and which would be helpful to sharpen the responsivities at both ends of the visible spectrum). By now the real TFD pixels are not mounted in a capture system with optics and camera body, but we expect that they will be in the next years. Also the use of sharpening filters within the visible range, like the color-optimum pre-filter proposed by Lyon and Hubel in [24], can very likely help in improving the TFD performance both in standard RGB mode and in the spectral recovery mode (multispectral capture system) proposed in this work. Also taking advantage of the results of this work, new TFD geometries can be designed to guarantee ab initio a lower overlap in the native spectral responses.

Conclusions

Our computations have shown that using the TFD with only two shots, a multispectral image can be captured with full spatial and spectral resolution. A set of five algorithms has been tested to recover spectral reflectances from these new generation reconfigurable sensor responses. Among the tested algorithms, the easiest to implement and to use is the Pseudoinverse method. However, it is not the best choice since its performance is very poor for noisy camera responses. Kernel yields the best results for all the metrics with the TFD responsivities, and also with an additional set of responsivities that are narrower spectrally. This shows that the TFD sensors performance in multispectral acquisition systems can be greatly increased if additional filters are introduced to make the responsivities narrower, without compromising the main advantages of the TFDs which are the tuneability and the full spatial resolution. This study offers a useful set of preliminary results confirming the applicability of this new detector technology in multispectral capture devices in the near future when the necessary improvements will be developed. In future work, we will substitute the pseudoinverse approach by the widely used Wiener algorithm, which is expected to perform better for noisy camera sensor responses.

References

[1] H. F. Grahn. P. Geladi, Techniques and Applications of Hyperspectral Image Analysis, John Wiley & Sons, Chichester, England, 2007, pg. 173.

[2] J. Kinnunen. S. Saarakkala. M. Hauta-Kasari. P. Vahimaa and J.S. Jurvelin. Optical spectral reflectance of human articular cartilage relationships with tissue structure. composition and mechanical properties, Biomedical Optics Express 2. 1394-1402 (2011).

[3] J.C. Noordam. W. H. A. M. van den Broek and L. M. C. Buydens, Detection and classification of latent defects and diseases on raw French fries with multispectral imaging, Proc. Agrotechnology and Food Innovations (A&F) Department Production & Control Systems. Wageningen. The Netherlands (2005).

[4] G. A. Shaw and Hsiao-Hua K. Burke, Spectral imaging for remote sensing, Lincoln Laboratory Journal 14. 3-28 (2003).

[5] M. L. Nischan. R. M. Joseph. J. C. Libby and J. P. Kerekes, Active spectral imaging, Lincoln Laboratory Journal 14. 131-144 (2003).

[6] F.H. Imai and R.S. Berns, Spectral estimation using trichromatic digital cameras, Proc. of the Internet. Symposium on Multispectral Imaging and Color Reproduction for Digital Archives. (Society of Multispectral Imaging of Japan). pp. 4248 (1999).

[7] J.P. Kerekes. J.R. Schott, Hyperspectral Imaging Systems, Hyperspectral Data Exploitation: Theory and Applications. C.I. Chang Ed. (John Wiley & Sons) (2006).

[8] M.A. Golub. et al, Spectral multiplexing method for digital snapshot spectral imaging, J. Applied Optics 48. 1520-1526 (2009).

[9] G. Langfelder. A. F. Longoni and F. Zaraga, Implementation of a multi-spectral color imaging device without color filter array, Proc. SPIE-IS&T 7876 787608/1 787608/9 (2011).

[10] G. Langfelder. F. Zaraga and A. Longoni, Tunable spectral responses in a color-sensitive CMOS pixel for imaging applications, Proc. IEEE 56. 2563-2569 (2009).

[11] V. Heikkinen. R. Lenz. T. Jetsu. J. Parkkinen. M. Hauta-Kasari and T. Jskelinen, Evaluation and unification of some methods for estimating reflectance spectra from RGB images, J. of the Optical Society of America A 25. 2444-2458 (2008).

[12] J. L. Nieves. E. M. Valero. J. Hernandez-Andres and J. Romero, Recovering fluorescent spectra with an RGB digital camera and color filters using different matrix factorizations, J. of Applied Optics 46. 4144-4154 (2007).

[13] N. Shimano. K. Terai and M. Hironaga, Recovery of spectral reflectances of objects imaged by multispectral cameras, J. of the Optical Society of America A 24. 3211-3219 (2007).

[14] S. M. C. Nascimento. F. P. Ferreira and D. H. Foster, Statistics of spatial cone-excitation ratios in natural scenes, J. of the Optical Society of America A 19. 1484-1490 (2002).

[15] M. J. Vhrel. R. Gershon. and L. S. Iwan, Measurement and analysis of object reflectance spectra, J. Color Research & Application 19. 49 (1994).

[16] J. L. Nieves. E. M. Valero. S. M. C. Nascimento. J. Hernandez-Andres. and J. Romero, Multispectral synthesis of daylight using a commercial digital CCD camera, J. of Applied Optics 44. 56965703 (2005).

[17] Y. Zhao. R.S. Berns, Image-Based Spectral Reflectance Reconstruction Using the Matrix R Method, J. Color Research & Application 32. 343-351 (2007).

[18] H. Stark, Vector Space Projections,John Wiley & Sons, England, 1998.

[19] M. D. Buhmann, Radial Basis Functions: Theory and Implementations, Cambridge University Press (2003).

[20] Y. Hu. J. Hernandez-Andres. J.L. Nieves. E.M. Valero. J. Romero. M. Schnitzlein and D. Nowack, Evaluation and optimization of spectral estimation algorithms for printer inks, Proc. AIC 2011 Interim Meeting (AIC). pp. 422-426 (2011).

[21] J. Romero. A. Garcia-Beltran. J. Hernandez-Andres, Linear bases for representation of natural and artificial illuminants, J. of the Optical Society of America A 14. 10071014 (1997).

[22] M. A. Lopez-Alvarez. J. Hernandez-Andres. E. M. Valero and J. L. Nieves, Colorimetric and Spectral Combined Metric for the Optimization of Multispectral Systems, Proc. 10th International Meeting of the AIC. 1685-1688 (2005).

[23] D. M. Allen, The relationship between variable selection and data augmentation and a method for prediction, J. Technometrics 16. 125-127 (1974).

[24] R. F. Lyon and P. M. Hubel, Eyeing the Camera: into the Next Century, Proc. IS&T/SID 10th Color Imaging Conf.. 349-355 (2002).

Author Biography

Miguel Angel Martinez received his BSc. in Telecomunications Engineering, Image and Sound at the University of Malaga, Spain (2007). He is currently researching for his MSc. thesis in Erasmus Mundus Master CIMET (2010-2012). His field of research has been colorimetric and Spectral performance of Tranverse Field Detectors at the Department of Optics of the University of Granada, Spain in collaboration with Politecnico di Milano, Italy.

Eva M. Valero obtained a B.D. in Physics in 1995, and a Ph.D. in 2000, both at the University of Granada. She has worked at the Department of Optics as assistant proffesor since 2001, and associate professor since 2007. Shes a member of the Color Imaging Lab at the University of Granada. Her research interests were initially spatial color vision, and more recently multispectral imaging and color image processing.

Giacomo Langfelder received the Ph.D. degree in 2009 from the Politecnico di Milano, Italy, where he is currently Assistant Professor with the Department of Electronics and Information Technology. His research focuses on radiation detectors and MEMS devices, with related frontend electronics. He is the author of more than 40 publications on refereed scientific journals and he is the co-inventor of patents on a novel color-sensitive detector and on new methods for image processing.

Javier Hernandez-Andres obtained his Ph.D. in 1999. Since 2003 he is Associate Professor at the Optics Department (University of Granada) and a member of its Color Imaging Lab. His research interests focus on multispectral imaging, science and technology. He is currently topical editor for the Journal of Optiscal Society of America A and member of the editorial board of the European Journal of Physics.